energies

MDPI

Article

Improving Thermal Stability and Hydrophobicity of Rutile-TiO_2 Nanoparticles for Oil-Impregnated Paper Application

Mohammed Mahmood Katun [1,*], Rudo Kadzutu-Sithole [2,*], Nosipho Moloto [2], Cuthbert Nyamupangedengu [1,*] and Chandima Gomes [1,*]

[1] School of Electrical and Information Engineering (EIE), Faculty of Engineering and the Built Environment(EBE), University of the Witwatersrand, Private Bag 3, Johannesburg 2050, South Africa
[2] Molecular Science Institute, School of Chemistry, University of the Witwatersrand, Private Bag 3, Johannesburg 2050, South Africa; nosipho.moloto@wits.ac.za
* Correspondence: mahmood.mohammed1@students.wits.ac.za (M.M.K.); rudo.sithole@wits.ac.za (R.K.-S.); cuthbert.nyamupangedengu@wits.ac.za (C.N.); chandima.gomes@wits.ac.za (C.G.)

Abstract: Thermal stress and moisture absorption can cause a synergetic negative impact on kraft paper. Among various approaches for improving the dielectric properties of kraft paper, nanotechnology has had promising results. However, the hydrophilicity of most metal oxide nanoparticles renders nanomodified kraft paper more vulnerable to thermal stress and moisture, thereby inducing degradation. In nanomodified kraft paper research, the use of TiO_2 nanoparticles has yielded the most promising results. The major shortfall, however, is the hydrophilicity of TiO_2. This work investigated surface modifications of rutile-TiO_2 nanoparticles (NPs) for improved hydrophobicity and thermal stability. Rutile-TiO_2 NPs is a nontoxic metal oxide that can withstand high temperature and is stable in chemical reactions. Two cases of surfactants were used—alkyl ketene dimer (AKD) and alkenyl succinic anhydride (ASA). The intention was to increase heat resistance and reduce the surface free energy of the rutile-TiO_2 NPs. The impacts of the surface modifiers on the rutile-TiO_2 NPs were characterised using FT-IR, muffle furnace, analytical weight balance, and TGA. It was discovered that new functional groups were formed on the modified NPs examined through FT-IR spectra. This indicates new chemical bonds, introduced through the surface modification. The unmodified rutile-TiO_2 NPs absorbed moisture, increasing their mass by 3.88%, compared with the modified nanoparticles, which released moisture instead. TGA analysis revealed that AKD- and ASA-modified rutile-TiO_2 needed higher temperatures than the unmodified rutile-TiO_2 to markedly decompose. AKD, however, gave better performance than ASA in that regard. As an example, those modified with 5% AKD sustained a 45% higher temperature than the pure TiO_2 nanoparticles. Furthermore, in both cases of the surfactants, the higher the percent of surfactant content was, the more thermally stable the nanoparticles became. This work demonstrates the possibility of fabricating rutile-TiO_2 NPs to give improved hydrophobicity and thermal stability for possible dielectric applications such as in kraft paper for power transformer insulation.

Keywords: transformer; cellulose; kraft paper; dielectric properties; thermal stability; moisture absorption; hydrophilic; nanoparticles; AKD; ASA; rutile-TiO_2

Citation: Mahmood Katun, M.; Kadzutu-Sithole, R.; Moloto, N.; Nyamupangedengu, C.; Gomes, C. Improving Thermal Stability and Hydrophobicity of Rutile-TiO_2 Nanoparticles for Oil-Impregnated Paper Application. *Energies* **2021**, *14*, 7964. https://doi.org/10.3390/en14237964

Academic Editor: Łukasz Nagi

Received: 16 August 2021
Accepted: 14 October 2021
Published: 29 November 2021

1. Introduction

Temperature rise in power transformers can cause thermal-induced degradation of kraft paper insulation. The temperature rise in power transformers may result from electrical faults, overloads, etc. [1,2].

Exposed hydroxyl sites on kraft paper (adsorption sites of cellulose) make it hygroscopic. The exposed site (OH) with a large dipole moment attracts water through the Coulomb force. The presence of water, therefore, modifies the dielectric properties of kraft

paper [3–7]. Such a compromised kraft paper suffers from accelerated decomposition. Associated problems include increased dielectric loss (loss factor) and increased susceptibility to partial discharge-induced degradation. Furthermore, the mechanical properties of kraft paper are degraded.

In a power transformer, the effects of pyrolysis and hydrolysis on kraft paper insulation cannot be treated independently, as the presence of one can influence the other. For instance, temperature rise in transformers can lead to moisture presence due to oxidation and can also distort the bonding structure of kraft paper. On the other hand, the presence of moisture in the transformer mostly due to ingress from the atmosphere or natural gassing of the transformer oil affects the hydrogen bond of kraft paper [8–12]. The hydrogen bond defines the cross linkage of cellulose chains on which the dielectric properties of the insulation depend [13,14]. In essence, therefore, the rate of thermal stability or withstand of kraft paper insulation is proportional to its moisture content [15].

To improve on kraft paper's thermal stability, normally the paper is either chemically or physically modified. Manufacturers of transformer insulation introduced different thermally upgraded kraft papers around the late 1950s. The National Electrical Manufacturers Association (NEMA) recognised these improvements in 1962 through the standard TR-1-1962 [16]. For the chemical modification of kraft paper, the water-absorbing group (hydroxyl group) of the cellulose which is vulnerable to thermal effect is replaced with a more stable functional group, cyanide ethylation patented in the early 1960s, as well as acetylation. As for physical modification (thermal stabilisers), the rate of insulation degradation is retarded through the reaction of the additives with degrading factors. Amine compounds are the most frequently used additives for physical modification [2,16–18].

According to Jusneret et al. [2] and Liang et al. [18], both chemical and physical approaches to thermal modification of cellulose increase the risk to health and safety of personnel, as well as environmental contamination. There is a possibility of discharge of highly toxic degradation by-products during thermal ageing, coupled with the displacement of hydrogen bonds, resulting in a decrease in mechanical strength. These setbacks are mainly due to cyanoethylation of kraft paper and the discharge of ammonia due to amino compounds. In the literature, therefore, there is always emphasis on the need to continuously search for less toxic and environmentally friendly kraft paper, with thermal endurance solutions. In that regard, this work was conceived to explore possibilities of improving the thermal stability of kraft paper through less toxic means.

In power transformers, more than 98% of the moisture is contained within kraft paper. To mitigate this, kraft paper is dried to reduce the moisture content to 0.5% (by dry weight), then impregnated with an oil to fill the air voids within the structure. When a transformer is in use, moisture is contained in the solid insulation, dissolved in oil, and also in a form of liquid in the core or bottom of the transformer [4,8,19–24]. The IEEE C57.140 Guide for Evaluation and Reconditioning of Liquid Immersed Power Transformer recommends drying wet insulation (solid and liquid). Some of these power transformer drying (maintenance) methods include factory drying, vacuum dry-out method, off-line processing approach, and the on-line transformer dryer [15,23]. According to a CIGRE working group A2.18 [24], migration of moisture from kraft paper to oil for extraction depends on temperature, and this process could take months. It follows, therefore, that moisture management in power transformers requires mitigating the rate of moisture absorption of kraft paper.

In this paper, the possibility of improving the thermal stability of a kraft paper with less toxic material, as well as controlling its vulnerability to the surrounding moisture, is explored. In the literature, nanotechnology has been recognised as a promising technique for improving the dielectric properties of kraft paper. However, regarding the hydrophilicity and thermal stability challenges of kraft paper, there has not been much research on using the technology as a possible solution.

In power transformer technology, the application of nanotechnology is increasingly drawing research attention as a promising tool in addressing major threats to the life of transformer insulation [25]. Kraft paper modified with nanoparticles has been reported to contain more hydrogen bonds, as more traps within cellulose structure are filled with the particles; this improves the bonding strength and the dielectric properties [26].

According to Liao et al. [27], oil-impregnated kraft paper modified with nano-TiO_2 prevents the injection of space charge distortion; a 50% decrease was reported for the modified paper with TiO_2 NPs. Liu et al. [28] improved surface discharge inception voltage on kraft paper modified with nanoparticles. The inception voltage was reported to have improved from 2.85 kV for an unmodified paper to 3.5 kV for the modified one. Hollertz [29] reported a 66% improvement in the tensile strength of paper after modification with nanoparticles. Among the nanoparticles used for modification of kraft paper, metal oxides are commonly used, and these include TiO_2, ZnO, SiO_2, and Al_2O_3 [7,26,28–30].

Of the options, nano-TiO_2 has been reported to be superior. Its compatibility and ability to improve the performance of kraft paper are notable. TiO_2 is reported to be more stable in reactions, nontoxic, low cost, and can withstand higher temperatures. The rutile phase of nano-TiO_2 has high electrical resistivity, thermal stability, and good mechanical strength. In contrast to the other common phases of the TiO_2 NPs (brookite and anatase), the rutile is chemically stable and can withstand very high temperatures and pressure without transforming or easily decomposing. Rutile-TiO_2 has a relatively high dielectric constant, making it suitable for some dielectric applications [31–37]. Although TiO_2 NPs are an attractive nanofiller for kraft paper, it has a major weakness in being hydrophilic [7,38,39]. It is worth noting that in the literature, most studies on modifying kraft paper with TiO_2 have been with the anatase phase and not the rutile. Therefore, in this work, the investigated nanoparticles were rutile-TiO_2. This paper presents a fabrication procedure that produced rutile-TiO_2 NPs with improved hydrophobicity and thermal stability.

2. Using Sizing Agents in Making Cellulose Fibre to Be Hydrophobic

Alkyl ketene dimer (AKD) and alkenyl succinic anhydride (ASA) are usually used to make organic compounds to be hydrophobic. They are the most used water-resistive agents (sizing) for manufacturing paper. Application of the sizing agent reduces the surface free energy of the host material, resulting in better hydrophobicity. The mechanism involves anchoring the hydrophilic head of the agents (AKD and ASA), with the host material and the hydrophobic tail extended out to repel water, as demonstrated in Figure 1. As far back as the 1960s, AKD and ASA have been used to control the wettability of paper. The extent of the interaction of the agents with the host determines the degree of resultant hydrophobicity of the modified paper [40–42].

Seppanen [43] used AKD and ASA to control the wettability of a paper and reported that the contact angle (angle with which the water makes with the paper surface) indicated a reduction in surface energy of the paper due to the application of the sizing agents. Hubbe [41] also reviewed studies in the literature on the application of internal sizing agents and revealed that AKD and ASA are the commonly used agents by paper manufacturers. It has also been reported that AKD and ASA increase the heat resistance of the resultant modified polymers and in cases where nano-metal oxides are used [40,41,43–49]. In this work, therefore, rutile-TiO_2 NPs were surface conditioned with AKD and ASA to study the effectiveness of the modification on thermal and hydrophilic properties of the resultant nanofiller. In the future extension of the present work, the modified TiO_2 NPs will be used to modify kraft paper for improved hydrophobicity and thermal stability.

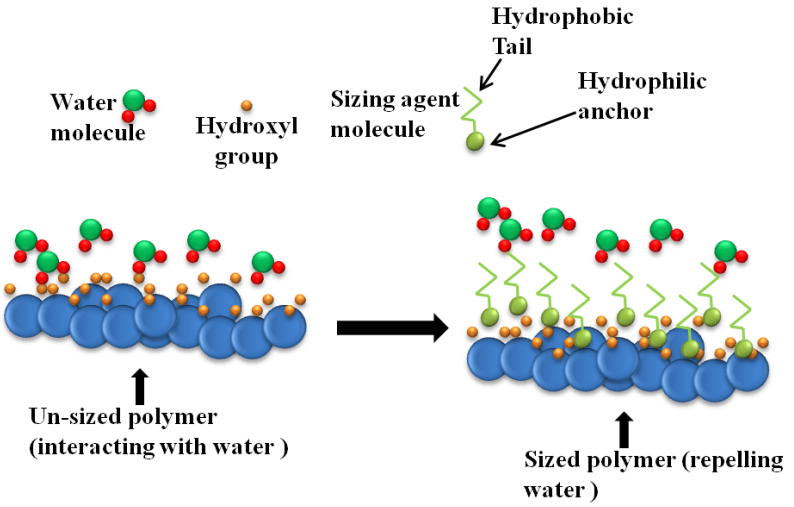

Figure 1. Sizing agent molecules orientation, redrawn from [50].

Bonding of inorganic fillers such as TiO_2 NPs with an inorganic sizing agent can be difficult. A coupling agent is, therefore, often used to bond the two. The coupling agent can be represented by the formula R $(CH_2)_n$ SiX_3. The 'X' is the hydrolysable group which forms a bond with TiO_2 NPs. 'R' is the functional group; it bonds with the polymer (cellulose) or organic material, which, in this case, are the sizing agents. Figure 2 illustrates the interface bonding of organic (sizing agents) and inorganic (TiO_2 NPs) material with silane. The nanofiller reacts with 'X' to produce silanol (forming metal hydroxide), while 'R' produces a covalent bond with organic material [39,50–54].

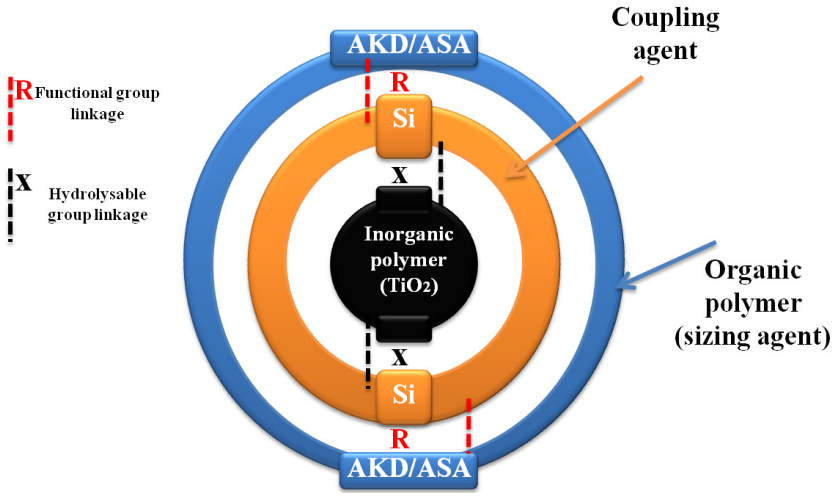

Figure 2. Silane interface bonding, redrawn from [51].

The rest of this paper presents the experimental work conducted to synthesise the rutile-TiO_2 NPs of specific shapes and dimensions. Some of the resultant nanoparticles were surface modified with AKD and others with ASA sizing agent. Both sets were then characterised using various techniques, and the results were analysed.

3. Experimental Procedures

3.1. Materials

AKD sizing agent emulsion was obtained from Sappi™ Technology Centre (Pretoria, South Africa). The ASA, silane coupling agent, and titanium (IV) butoxide were purchased from Sigma-Aldrich (Pty.) Ltd. (St. Louis, MO, USA). Both chemicals were used as received.

3.2. Synthesis of Rutile-TiO_2 Nanoparticles

The sol–gel method was used to synthesise rutile-TiO_2 nanoparticles. The synthesis procedure was iteratively explored to target producing rutile-TiO_2 NPs of less than 20 nm. The resultant optimised procedure is summarised as follows: a total of 30 mL titanium butoxide ($Ti(OBu)_4$) was added dropwise into 30 mL ice-water in a glass beaker under magnetic stirring. The resultant aqueous solution was stirred for 30 min and heated to remove water. A white residue was obtained, sonicated, and then washed several times in distilled water before centrifuging. The product was dried in a laboratory oven at 80 °C for 24 h. 500 mg of the dry powder was annealed in a muffle furnace at 700 °C, ramped for 2 h, and held for 2 h, resulting in the formation of the rutile phase of TiO_2. The resultant NPs were determined to be 19.7 nm on average. The NPs synthesis procedure is illustrated in Figure 3. The synthesised nanoparticles were surface modified, as presented in the next section.

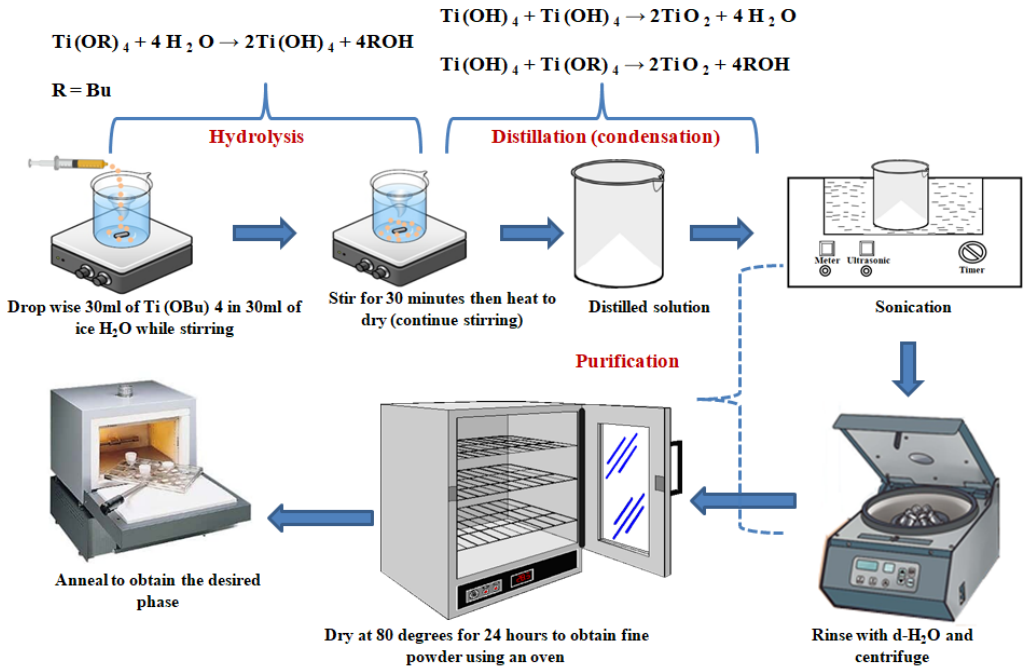

Figure 3. Schematic illustration of synthesising rutile-TiO2 NPs.

3.3. Surface Modification of the Rutile-TiO_2 Nanoparticles

Three portions of 10 g each of TiO_2 nanoparticles were dispersed in 32 mL of distilled water and sonicated for 30 min. Then, 5 vol/vol%, 3 vol/vol%, and 1 vol/vol% of AKD were added, making samples X, Y, and Z. The same procedure was repeated for ASA, making samples A, B, C. After 35 min of stirring, 1.5 vol/vol% silane was added to each mixture to connect the dissimilar compounds together and was stirred for 1 h. For ASA, alum was added to the solution to further fuse and retain the ASA with the TiO_2. Both mixtures were heated for 20 min at 60 °C with continued stirring. The obtained samples were centrifuged and rinsed with distilled water to remove the impurities and dried at 80 °C. Figure 4 shows the block illustration of the modification model. The reaction mechanism model is illustrated in Figure 5. The hydrolysis of the silane (Si-OH) makes

TiO_2 NPs react with the hydrolysable group ($Si(OH)_3$), while the organofunctional group reacts with sizing agents (AKD and ASA).

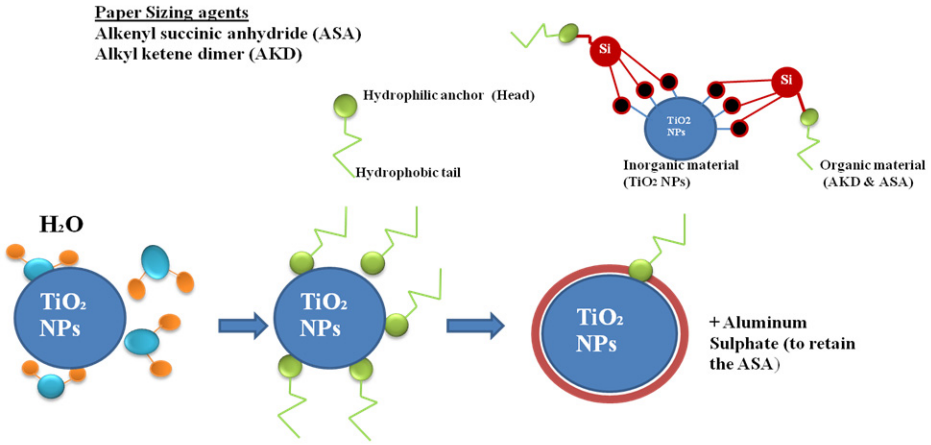

Figure 4. An illustration of surface modification concept of rutile-TiO_2.

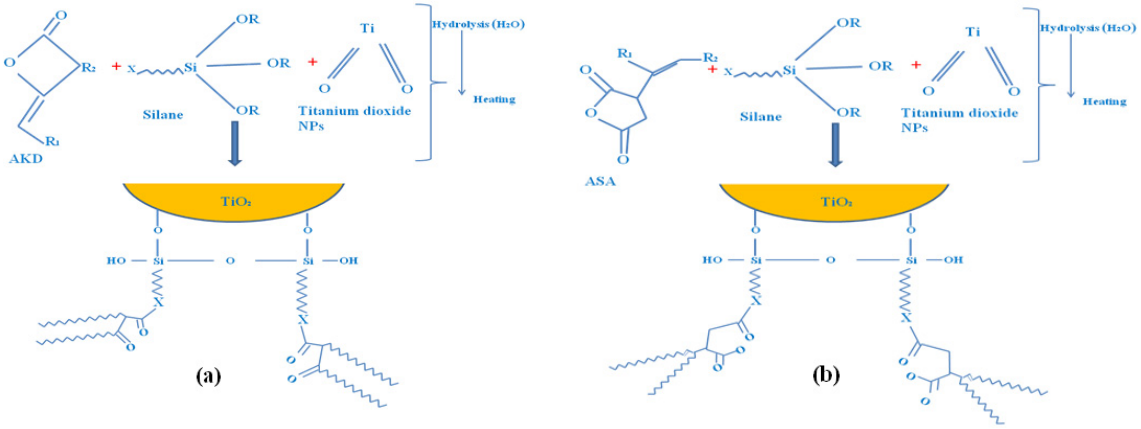

Figure 5. Reaction mechanism model: (**a**) TiO_2 NPs/AKD; (**b**) TiO_2 NPs/ASA.

4. Characterisation of the Surface-Modified Rutile-TiO_2 Nanoparticles

Phase identification of the sample was conducted using X-ray diffraction (Bruker MeasSrv (D2-205530)/D2205530 diffractometer), as well as with Raman spectroscopy using Bruker Infinity 1 spectrometer (Billerica, MS, USA) fitted with a 50× objective lens for imaging. The nanoparticles shape was identified using transmission electron microscopy (TEM). The Fourier-transform infrared spectroscopy (FT-IR) spectra of the samples were obtained with an attenuated total reflectance (ATR) in the wavelength range of 420–4000 cm^{-1} using PerkinElmer [55]. Analytical weight balance was used to measure changes in mass of the sample due to moisture absorption and heat. A thermogravimetric analyser (PerkinElmer STA 4000 analyser; Waltham, MA, USA) was used to study the thermal stability of the samples. The various results of each analysis are presented in the next section.

4.1. X-ray Diffraction Results

X-ray diffraction (XRD) was used to determine the crystallinity and phase of the synthesised TiO_2 NPs. The XRD pattern shows distinct diffraction peaks which match the standard rutile-TiO_2 reference peaks. All peaks are in good agreement with the standard spectrum (JCPDS no.: 88-1175). As shown in Figure 6, the diffraction depicts sharpness of the peaks, which indicates highly crystalline nanoparticles [56–58].

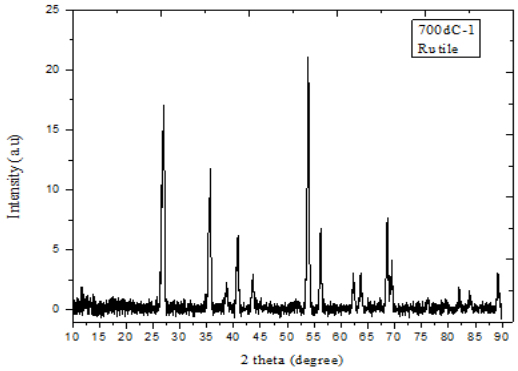

Figure 6. X-ray diffraction pattern of the obtained rutile-TiO_2 NPs.

The average crystallite size of the obtained rutile-TiO_2 nanoparticles was calculated to be 19.7 nm. The size was determined by the use of the Scherrer equation (Equation (1)) [56] as given in Equation (1).

$$S = \frac{K\lambda}{L\cos\theta} \quad (1)$$

where

S = crystallites diameter (nm);
K = 0.9 (Scherrer constant);
λ = 0.14506 (wavelength of the X-ray source);
L = full width-half maximum radians (FWMH);
θ = peak position.

4.2. Raman Spectroscopy Results

Raman spectroscopy was used to characterise the obtained rutile-TiO_2 NPs. Four random spots were scanned on the specimen. The spectrum in Figure 7 shows the Raman peak shifts for the rutile-TiO_2 NPs. The rutile-TiO_2 has four characteristic phonon modes at 143 ± 2 cm^{-1} (B_{1g}), 445 ± 5 cm^{-1} (E_g), 610 ± 1 cm^{-1} (A_{1g}), and 235 ± 5 cm^{-1}. From Figure 7, it is evident that rutile exhibits dominant peaks at 448.16 cm^{-1} and 611.04 cm^{-1}. These peaks are attributed to E_g and A_{1g}, active modes of rutile-TiO_2 correspondently. The third-most active optical phonon mode of rutile from the graph is the 144.06 cm^{-1} which is attributed to B_{1g}. The peak at 825.16 cm^{-1} is the weakest and poorly observed. This peak is assigned B_{2g}. A visible broadband at 235.76 cm^{-1}, as observed on the graph, does not correspond with any fundamental modes of the rutile phase. This may be attributed to the disorder-induced scattering or second-order effect (SOE) as a consequence of multi-phonon processes [59–61].

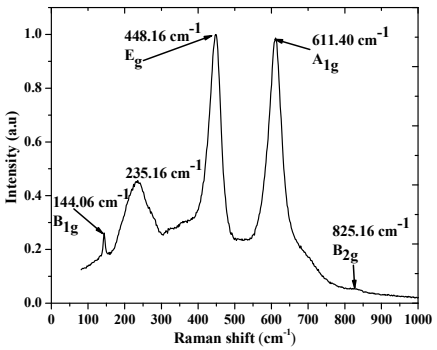

Figure 7. Raman spectrum of the obtained rutile TiO_2 NPs.

4.3. Transmission Electron Microscopy (TEM) Results

Transmission electron microscopy (TEM) was used to examine the samples' morphology and size. As shown in Figure 8, the particles are agglomerated; therefore, particle size distribution cannot be ascertained from the images obtained. However, as earlier reported in the XRD analysis using the Scherrer equation, the average size of nanoparticles was calculated as 19.7 nm. The agglomeration obtained in the particles could be due to the high temperature used during calcination (which exists between the transition of the two polymorphous of TiO_2). Additionally, for small particles, Van der Waals attraction force that is present between the NPs leads to agglomeration [60–63]. From the TEM images, hexagonal-like shape is evident. To reduce agglomeration, high shear force mixing, ball milling, or ultrasonication has to be employed for mixing with the host polymer such as the case of kraft paper [64].

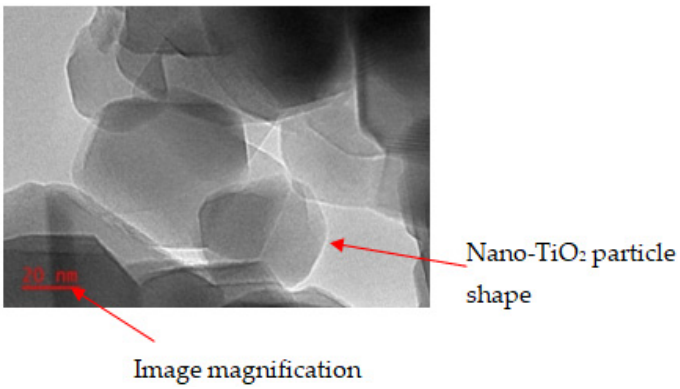

Figure 8. TEM images of the obtained rutile-TiO_2 NPs.

4.4. Fourier-Transform Infrared Spectroscopy (FT-IR)

The FT-IR was recorded at room temperature using a PerkinElmer Fourier-transform-attenuated total reflectance–infrared spectrometer (FT-UATR-IR-2) in the range from 420–4000 cm^{-1}. As shown in Figure 9a, the spectrum of the obtained sample (rutile-TiO_2) was examined and compared with what is in the literature. The appearance of a band in the region 531 cm^{-1} of the TiO_2 NPs spectrum indicates the presence of metal to oxygen bonding which corresponds to O-Ti-O bonding [64–69]. Compared with what is available in the literature, the characteristic of -OH group (3200–3650 cm^{-1}) is not obvious in the TiO_2 spectrum [69–73]. This could be due to the annealing temperature and time, leading to the removal of hydrolysable surface group, thereby fabricating ligand-free TiO_2 NPs [74–76].

The FT-IR of the modified TiO_2 NPs was conducted to examine the spectra of each sample. Figure 9b shows the FT-IR spectra of pure AKD. From the plot, a weak and broad peak is evident between 3041 and 3565 cm^{-1} which is characteristic of (OH) vibrations in the AKD spectrum [77]. Comparing Figure 9b,c of the modified TiO_2 NPs, the modified TiO_2 NPs show the presence of AKD features on its structure. The double bond carbon–carbon stretching vibration–absorption peak at 1708 cm^{-1} relates to the absorption band characteristic peak 1846 and 1633 cm^{-1} in the spectrum of AKD which usually correspond to C=O and C=C. However, there was an absence of OH frequency absorption band in the modified TiO_2 NPs, suggesting the dehydration of water molecules in the complexes. The appearance of double bond carbon stretching at 1708 cm^{-1} is very weak (almost not existing). This indicates that the functional group is very symmetrical but does not imply that the functional group is absent.

The adsorption bands at 2849 and 2916 cm^{-1} of the modified TiO_2 NPs are from –CH2-symmetric and asymmetric stretching vibration [48]. The spectra of the modified TiO_2 NPs with AKD, therefore, shows that new absorption bands are present which is evidence of the presence of new chemical bonds formed through modification. There is a reaction and connection between TiO_2 NPs and AKD.

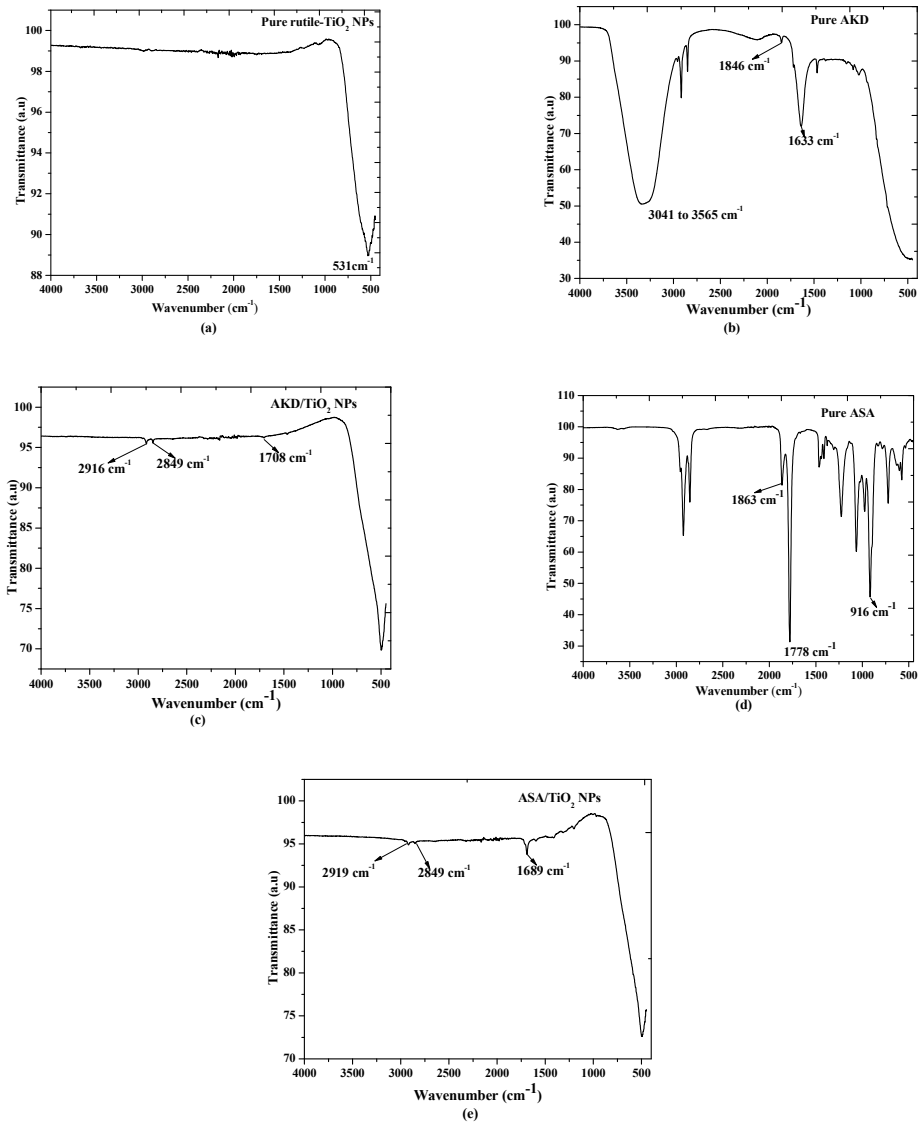

Figure 9. Fourier-transform infrared spectra: (**a**) pure rutile-TiO_2 NPs; (**b**) pure AKD; (**c**) AKD surface-modified rutile-TiO_2 NPs; (**d**) pure ASA; (**e**) ASA surface-modified rutile-TiO_2 NPs.

The FT-IR spectrum of ASA is shown in Figure 9d. The spectrum peaks for ASA arising from anhydride carbonyl stretching were identified at 1778 cm^{-1} and 1863 cm^{-1} which correspond with the literature. The 1778 cm^{-1} represents the stretching vibration of C=O which conforms with 1785 ± 5 cm^{-1}. At 916 cm^{-1}, the stretching vibration band of five-membered cyclic anhydrides (succinic anhydride) is identified. In Figure 9e which characterises the modified TiO_2 NPs with ASA, there is an absence of succinic anhydride grouping (1778 cm^{-1} and 1863 cm^{-1}). This is due to the hydrolysis of the anhydride which results in the appearance of a band at 1689 cm^{-1}. The band corresponds to the stretching vibration of the C=O bond [78–80]. The absence of the bands at 1863 to 1778 cm^{-1} indicates that the composite is free of unreacted modifier (ASA).The adsorption bands at 2849 and 2919 cm^{-1} of the modified TiO_2 NPs are also from –CH2- symmetric and asymmetric stretching vibration [48]. Figure 9e, therefore, demonstrates that new adsorption bands and chemical bonds are formed after modification.

4.5. Moisture Absorption Characteristics

Each sample of the surface-modified TiO_2 NPs, including the unmodified, was weighed using an analytical weigh balance. Then, 10 mL of distilled water was dropped in each sample and was exposed to air for 3 days. The experiment was triplicated; the average values and the error deviations are summarised in Table 1.

Table 1. Change in mass due to absorbed moisture.

Sample	Sample Mass (mg)	Average Triplicated Sample Mass after 3 Days Exposure to Moisture	Mass Change (%)
T (unmodified)	500	519.40 ± 0.46	3.88 ± 0.09
A (5%ASA)	500	494.40 ± 0.62	−1.12 ± 0.12
B (3%ASA)	500	497.00 ± 0.36	−0.60 ± 0.07
C (1%ASA)	500	497.70 ± 0.70	−0.46 ± 0.14
X (5%AKD)	500	486.70 ± 0.20	−2.66 ± 0.04
Y (3%AKD)	500	492.30 ± 0.44	−1.54 ± 0.09
Z (1%AKD)	500	494.00 ± 0.30	−1.20 ± 0.06

The unmodified rutile-TiO2 NPs (sample 'T'), after having been exposed to air-absorbed moisture, had a weight increase of 3.88%. In contrast, the modified samples generally lost weight by releasing water into the atmosphere. These results demonstrate the hydrophilic nature of TiO_2 and the effect of sizing agents on reducing the hydrophilicity behaviour of TiO_2.

4.6. Thermal-Stress-Induced Weight Loss of Surface-Modified Rutile-TiO_2 NPs

To determine thermal-stress-induced weight loss characteristics, 300 mg portions of each sample were measured separately and placed in a furnace. The furnace temperature was set to ramp up to 400 °C in 20 min and then stayed constant for 40 min. The samples were then placed in a desiccator with silica gel to avoid moisture absorption as the samples cooled off. Analytical weight balance was used to measure the change in mass of each sample. This experiment was triplicated; Table 2 shows the average value of the weight loss and error deviation of each case.

Table 2. Weight loss analysis of surface-modified rutile-TiO_2 NPs under thermal stress.

Sample	Sample Initial Mass (mg)	Average Triplicated Sample Mass after 3 Days	Weight Loss (%)
T (unmodified)	300	298.80 ± 0.78	0.40 ± 0.26
A (5%ASA)	300	293.00 ± 0.50	2.33 ± 0.17
B (3%ASA)	300	292.30 ± 0.61	2.57 ± 0.21
C (1%ASA)	300	291.50 ± 0.50	2.83 ± 0.17
X (5%AKD)	300	295.60 ± 0.53	1.47 ± 0.18
Y (3%AKD)	300	296.70 ± 0.20	1.10 ± 0.07
Z (1%AKD)	300	297.20 ± 0.36	0.93 ± 0.12

From the table, the surface-modified samples lost more weight than the unmodified sample, and the amount of weight loss is directly proportional to the percent content of the sizing agent applied on each sample. The weight loss of the composites can be attributed to the breakage or disintegration of the bond between organic and inorganic compounds [81]. This indicates that the modified samples contain more than one compound. In essence, the weight loss under heating is predominated by the decomposition of the surfactants. This phenomenon is further confirmed in the thermogravimetric analysis, as presented in the next section.

4.7. Thermogravimetric Analysis (TGA) Results

The Thermogravimetric analysis (TGA) of the samples was conducted under nitrogen gas. From the graph of pure TiO_2 NPs (Figure 10a), a rapid loss of moisture occurred between 75 and 90 °C, followed by a significant degradation at about 186 °C which is attributed to the decomposition of the TiO_2 [45,82]. The initial steep gradient (representing a rapid loss of moisture) and the subsequent steep depression on the graph further confirm the results obtained in Table 1 about moisture absorption of the unmodified sample. As for the 5% AKD-modified rutile-TiO_2 NPs, there is drastic thermal decomposition at 270 °C which is about 45% higher than that of pure rutile-TiO_2 NPs. For the reduced AKD content of 3%, the decomposition of modified rutile-TiO_2 NPs occurs at a lower temperature of 261 °C which is about 40% higher than that of the pure rutile-TiO_2 NPs. A further reduction of AKD to 1% resulted in the modified rutile-TiO_2 NPs decomposing drastically at 253 °C which is about 36% higher than that of pure rutile-TiO_2 NPs. For AKD, in all cases of surface medication of rutile-TiO_2 NPs, there is increased thermal stability of at least 36%. In the case of ASA modified NPs, the temperatures at which the modified NPs drastically decomposed were 211 °C, 194 °C, 187 °C for 5%, 3% and 1% ASA content, respectively. It is worth noting that for all cases of ASA modification, the temperature at which drastic decomposition occurred was lower than the least % AKD content modified sample. This shows that AKD modified samples are more thermally stable than the ASA. However, the ASA-modified samples show improvement in thermal stability except for 1% content whose thermal stability is the same as that of the pure rutile-TiO_2 NPs. Table 3 summarises the effects of surfactant content and type on the thermal stability of the resultant modified samples.

Table 3. Effects of surfactant content and type on thermal stability.

Sample	Temperature at Which Drastic Decomposition Occurred (°C)	Difference in Temperature to the Pure Rutile-TiO2 NPs (%)
T (unmodified)	186	0
A (5%AKD)	270	45.2
B (3%AKD)	261	40.3
C (1%AKD)	253	36.0
X (5%ASA)	211	13.4
Y (3%ASA)	194	4.3
Z (1%ASA)	187	0.5

The decomposition of the modified rutile-TiO_2 NPs samples at higher temperatures could be attributed to improved heat resistance associated with the long-chain organic compounds from surfactants [57,79,82–84]. Both cases of the modified TiO_2 NPs show that the modified samples have better thermal stability than pure rutile-TiO_2 NPs.

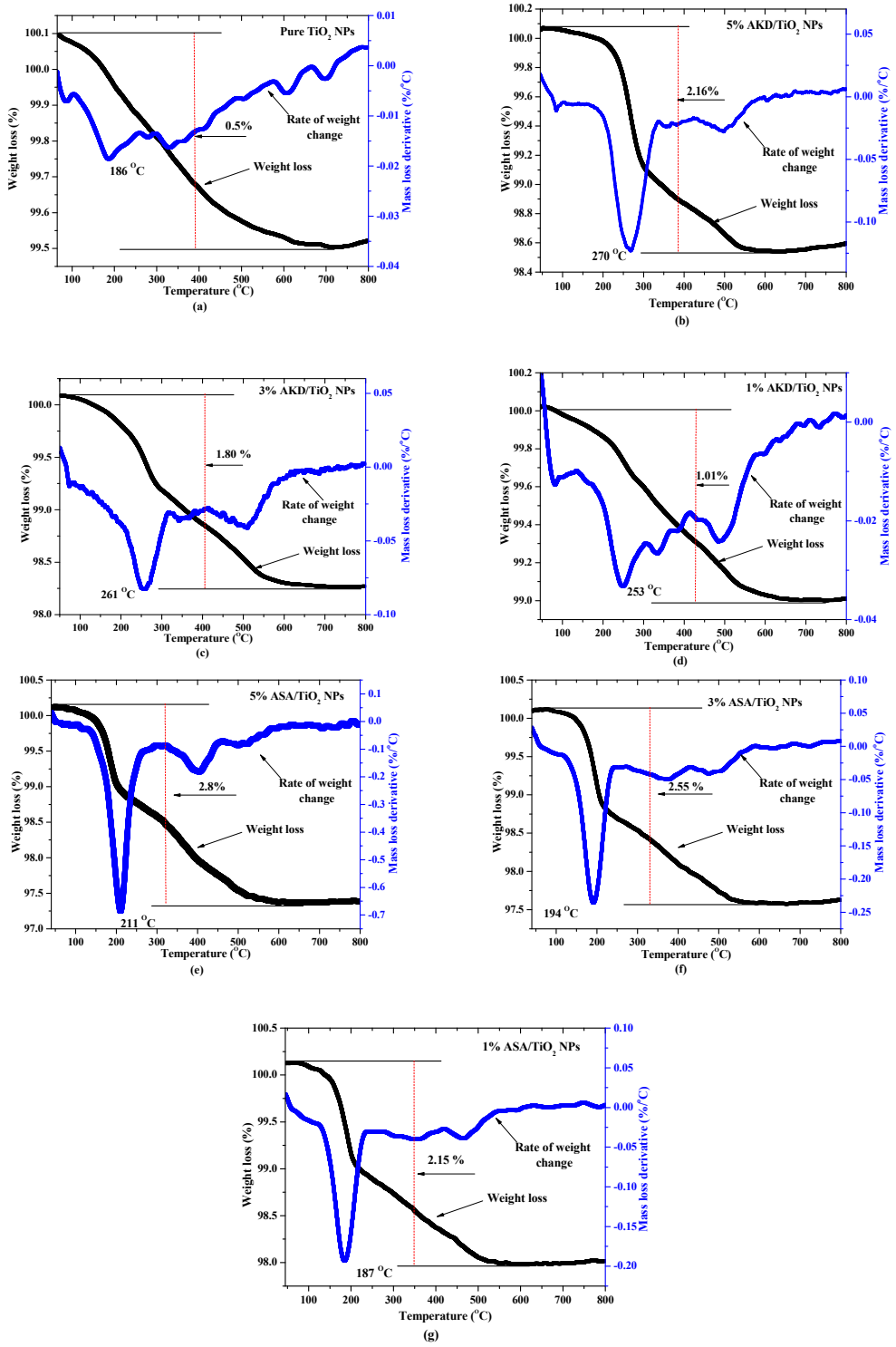

Figure 10. Thermogravimetric analysis graph: (**a**) pure TiO2 NPs; (**b**) 5% AKD/TiO_2 NPs; (**c**) 3% AKD/TiO_2 NPs; (**d**) 1% AKD/TiO_2 NPs; (**e**) 5% ASA/TiO_2 NPs; (**f**) 3% ASA/TiO_2 NPs; (**g**) 1% ASA/TiO_2 NPs.

5. Conclusions

A protocol to synthesise 19.7 nm rutile-TiO_2 NPs was proposed and presented in this work. It was further demonstrated that the moisture absorption characteristics, as well as thermal stability of the nanoparticles, can be improved through surface modification of the rutile-TiO_2 NPs. Two types of surfactants were investigated: AKD and ASA. In the case of AKD surface-modified rutile-TiO_2 NPs, the FT-IR spectra indicate the presence of new functional groups. Improvement in terms of rate of moisture absorption (within an approximate deviation of $\pm 0.14\%$) and thermal stability were determined in surface-modified rutile-TiO_2 NPs. For ASA surface-modified rutile-TiO_2 NPs, there was improvement observed in the rate of moisture absorption and thermal stability except for the least % content of ASA sample that behaved similar to the unmodified rutile-TiO_2 NPs. Possible applications of the more thermally stable and hydrophobic modified rutile-TiO_2 can be explored in future works.

Author Contributions: Conceptualisation, M.M.K., C.G. and C.N.; methodology, M.M.K. and R.K.-S.; validation, M.M.K., C.G., C.N. and R.K.-S.; formal analysis, M.M.K., CN and R.K.-S.; investigation, M.M.K.; writing—original draft preparation, M.M.K.; writing—review and editing, M.M.K., C.N. and R.K.-S.; supervision, C.G. and C.N.; resources, N.M. All authors have read and agreed to the published version of the manuscript.

Funding: This research received no external funding.

Institutional Review Board Statement: Not applicable.

Informed Consent Statement: Not applicable.

Data Availability Statement: Data is contained within the article.

Conflicts of Interest: The authors declare no conflict of interest.

References

1. Lisoň, L.; Kolcunová, I.; Kmec, M. Effect of Thermal Ageing on the Oil-Paper Insulation. *Acta Electrotech. Inform.* **2014**, *14*, 23–26. [CrossRef]
2. Jusner, P.; Schwaiger, E.; Potthast, A.; Rosenau, T. Thermal stability of cellulose insulation in electrical power transformers—A review. *Carbohydr. Polym.* **2021**, *252*, 117196. [CrossRef]
3. Oommen, T.V.; Prevost, T.A. Cellulose insulation in oil-filled power transformers: Part II maintaining insulation integrity and life. *IEEE Electr. Insul. Mag.* **2006**, *22*, 5–14. [CrossRef]
4. Anglhuber, M. Why is water killing power transformer insulation? *Transformers Magazine*, 8 July 2017; pp. 106–112.
5. Kulasinski, K.; Guyer, R.; Derome, D.; Carmeliet, J. Water Adsorption in Wood Microfibril-Hemicellulose System: Role of the Crystalline–Amorphous Interface. *Biomacromolecules* **2015**, *16*, 2972–2978. [CrossRef] [PubMed]
6. Kulasinski, K. Effects of Water Adsorption in Hydrophilic Polymers. In *Polymer Science: Research Advances, Practical Applications and Educational Aspects*; Formatex Research Center: Badajoz, Spain, 2016; pp. 217–223, ISBN 978-84-942134-8-9.
7. Nikjoo, R.; Taylor, N.; Edin, H.; Hollertz, R.; Wahlander, M.; Wagberg, L.; Malmstrom, E. Comparison of oil-impregnated papers with SiO2 and ZnO nanoparticles or high lignin content, for the effect of superimposed impulse voltage on AC surface PD. *IEEE Trans. Dielectr. Electr. Insul.* **2017**, *24*, 1726–1734. [CrossRef]
8. Gielniak, J.; Graczkowski, A.; Moranda, H.; Przybylek, P.; Walczak, K.; Nadolny, Z.; Moscicka-Grzesiak, H.; Feser, K.; Gubanski, S.M. Moisture in cellulose insulation of power transformers—Statistics. *IEEE Trans. Dielectr. Electr. Insul.* **2013**, *20*, 982–987. [CrossRef]
9. Martin, D.; Saha, T.; Dee, R.; Buckley, G.; Chinnarajan, S.; Caldwell, G.; Zhou, J.B.; Russell, G. Determining water in transformer paper insulation: Analyzing aging transformers. *IEEE Electr. Insul. Mag.* **2015**, *31*, 23–32. [CrossRef]
10. Prevost, T.A.; Oommen, T.V. Cellulose insulation in oil-filled power transformers: Part I—History and development. *IEEE Electr. Insul. Mag.* **2006**, *22*, 28–35. [CrossRef]
11. Garcia, B.; Burgos, J.C.; Alonso, A.M.; Sanz, J. A moisture-in-oil model for power transformer monitoring—Part I: Theoretical foundation. *IEEE Trans. Power Deliv.* **2005**, *20*, 1417–1422. [CrossRef]
12. Shroff, D.H.; Stannett, A.W. A review of paper aging in power transformers. *Transm. Distrib. IEE Proc. C-Gener.* **1985**, *132*, 312–319. [CrossRef]
13. Przybysz, P.; Dubowik, M.; Kucner, M.A.; Przybysz, K.; Przybysz Buzała, K. Contribution of Hydrogen Bonds to Paper Strength Properties. *PLoS ONE* **2016**, *11*, e0155809. [CrossRef]
14. Hirn, U.; Schennach, R. Comprehensive analysis of individual pulp fiber bonds quantifies the mechanisms of fiber bonding in paper. *Sci. Rep.* **2015**, *5*, 10503. [CrossRef]

15. Fofana, I.; Wasserberg, V.; Borsi, H.; Gockenbach, E. Drying of Transformer Insulation using Zeolite. *Electr. Insul. Mag. IEEE* **2004**, *20*, 20–30. [CrossRef]
16. Prevost, T.A. Thermally Upgraded Insulation in Transformers. In Proceedings of the IEEE Electrical Insulation Conference and Electrical Manufacturing Expo, Indianapolis, IN, USA, 23–26 October 2005. [CrossRef]
17. Morrison, E.L. Evaluation of the Thermal Stability of Electrical Insulating Paper. *IEEE Trans. Electr. Insul.* **1968**, *EI-3*, 76–82. [CrossRef]
18. Liang, N.; Liao, R.; Xiang, M.; Mo, Y.; Yuan, Y. Influence of Amine Compounds on the Thermal Stability of Paper-Oil Insulation. *Polymers* **2018**, *10*, 891. [CrossRef] [PubMed]
19. Cai, J.; Zhang, T. Moisture content assessment of transformer solid insulation using return voltage spectrum. In Proceedings of the 2009 IEEE 9th International Conference on the Properties and Applications of Dielectric Materials, Harbin, China, 19–23 July 2009; pp. 257–260. [CrossRef]
20. Martin, D.; Saha, T.; Perkasa, C.; Lelekakis, N.; Gradnik, T. Fundamental concepts of using water activity probes to assess transformer insulation water content. *IEEE Electr. Insul. Mag.* **2016**, *32*, 9–16. [CrossRef]
21. Cui, Y.; Ma, H.; Saha, T.; Ekanayake, C. Understanding Moisture Dynamics and Its Effect on the Dielectric Response of Transformer Insulation. *IEEE Trans. Power Deliv.* **2015**, *30*, 2195–2204. [CrossRef]
22. Suleiman, A.A.; Nazri, F.; Muhamad, N.A.; Bashir, N.; Mohamad, Z. Wetting characteristics for kraft paper immersed in mineral and biodegradable insulation oils. In Proceedings of the 2014 IEEE 8th International Power Engineering and Optimization Conference (PEOCO2014), Langkawi, Malaysia, 24–25 March 2014; pp. 194–198. [CrossRef]
23. IEEE. Guide for Evaluation and Reconditioning of Liquid Immersed Power Transformers. In *IEEE Std C57140-2017 Revis. IEEE Std C57140-2006*; IEEE: New York, NY, USA, 2017; pp. 1–88. [CrossRef]
24. CIGRE Working Group A2. *18. Life Management Techniques for Power Transformers*; CIGRE: Paris, France, 2003.
25. Contreras, J.E.; Rodríguez, E.; Taha-Tijerina, J. Nanotechnology applications for electrical transformers—A review. *Electr. Power Syst. Res.* **2017**, *143*, 573–584. [CrossRef]
26. Liu, D.; Ye, J.; Xu, X.; Deng, C.G.; Li, X. Optimization of Mass Fraction and Particle Size of TiO_2 Additives in Application of HVDC Transformer Insulation. In Proceedings of the 2019 IEEE 20th International Conference on Dielectric Liquids (ICDL), Roma, Italy, 23–27 June 2019. [CrossRef]
27. Liao, R.-J.; Lv, C.; Yang, L.; Zhang, Y.-Y.; Liu, T. Space Charge Behavior in Oil-Impregnated Insulation Paper Reinforced with Nano-TiO_2. *BioResources* **2013**, *8*, 5655–5665. [CrossRef]
28. Liu, D.; Wu, Y.; Xu, X.; Ye, J.; Li, J.; Yu, S.; Li, X. Suppression Mechanism of TiO2 for the Partial Discharge of Oil-Paper Insulation in Intensive Electric Field. In Proceedings of the 20th International Conference on Dielectric Liquids (ICDL), Rome, Italy, 23–27 June 2019. [CrossRef]
29. Hollertz, R.; Wagberga, L.; Pitois, C. Novel cellulose nanomaterials. In Proceedings of the 2014 IEEE 18th International Conference on Dielectric Liquids (ICDL), Bled, Slovenia, 29 June–3 July 2014; pp. 1–4. [CrossRef]
30. Liao, R.; Zhang, F.; Yuan, Y.; Yang, L.; Liu, T.; Tang, C. Preparation and Electrical Properties of Insulation Paper Composed of SiO2 Hollow Spheres. *Energies* **2012**, *5*, 2943–2951. [CrossRef]
31. Gao, F.; Xiang, M.; Liao, R.; Xu, Z.; Wang, J. The experimental investigation on space charge distribution of cellulose insulation paper modified with alumina nanoparticles. In Proceedings of the 2016 International Conference on Condition Monitoring and Diagnosis (CMD), Xi'an, China, 25–28 September 2016; pp. 757–760. [CrossRef]
32. Gomes, C.; Izadi, M. Electrical Isolation of Two Earthing Systems under Lightning Conditions with TiO_2 Nano Fluid Barrier. In Proceedings of the 2019 International Symposium on Lightning Protection (XV SIPDA), Sao Paulo, Brazil, 30 September–4 October 2019; pp. 1–5. [CrossRef]
33. Calva, P.; Cano, A.; Martinez, H. Fillers in Electrical Papers for Power Transformers. *Adv. Mater. Res.* **2014**, *875*, 335–340. [CrossRef]
34. Morsy, F.; El-sherbiny, S.; Samir, M.; Fouad, O. Application of nanostructured titanium dioxide pigments in paper coating: A comparison between prepared and commercially available ones. *J. Coat. Technol. Res.* **2015**, *13*, 307–316. [CrossRef]
35. Noman, M.T.; Ashraf, M.A.; Ali, A. Synthesis and applications of nano-TiO_2: A review. *Environ. Sci. Pollut. Res.* **2019**, *26*, 3262–3291. [CrossRef]
36. Diebold, U. The surface science of titanium dioxide. *Surf. Sci. Rep.* **2003**, *48*, 53–229. [CrossRef]
37. Malekshahi Byranvand, M.; Kharata, A.; Fatholahib, L.; Malekshahi Beiranvand, Z. A Review on Synthesis of Nano-TiO_2 via Different Methods. *J. NanoStruct.* **2013**, *3*, 1–9. [CrossRef]
38. Kapilashrami, M.; Zhang, Y.; Liu, Y.S.; Hagfeldt, A.; Guo, J. Probing the Optical Property and Electronic Structure of TiO_2 Nanomaterials for Renewable Energy Applications. *Chem. Rev.* **2014**, *114*, 9662–9707. [CrossRef] [PubMed]
39. Vorontsov, A.; Valdes, H.; Smirniotis, P.; Paz, Y. Recent Advancements in the Understanding of the Surface Chemis-try in TiO_2 Photocatalysis. *Surfaces* **2020**, *3*, 72–92. [CrossRef]
40. Andritsch, T.; Fabiani, D.; Vazquez, I. Nanodielectrics-examples of preparation and microstructure. *IEEE Electr. Insul. Mag.* **2013**, *29*, 21–28. [CrossRef]
41. Hubbe, M. Paper's resistance to wetting—A review of internal sizing chemicals and their effects. *BioResources* **2007**, *2*, 106–145.
42. Porkert, S. "Physico-Chemical Processes during Reactive Paper Sizing with Alkenyl Succinic Anhydride (ASA)," Technische Universität Dresden, Germany. 2016. Available online: http://rgdoi.net/10.13140/RG.2.2.18268.39045 (accessed on 9 November 2019).

43. Rauni, S. *On the Internal Sizing Mechanisms of Paper with AKD and ASA Related to Surface Chemistry, Wettability and Friction, KTH*; Royal Institute of Technology: Stockholm, Sweden, 2007.
44. Tsuda, Y.; Kojima, M.; Matsuda, T.; Oh, J.M. Soluble Polyimides Based on Long-chain Alkyl Groups via Amide Linkages. *Polym. J.* **2008**, *40*, 354–366. [CrossRef]
45. Biswas, A.; Cheng, H.N.; Kim, S.; Alves, C.R.; Furtado, R.F. Hydrophobic Modification of Cashew Gum with Alkenyl Succinic Anhydride. *Polymers* **2020**, *12*, 514. [CrossRef]
46. Ryu, Y.S.; Lee, J.H.; Kim, S.H. Efficacy of alkyl ketene dimer modified microcrystalline cellulose in polypropylene matrix. *Polymer* **2020**, *196*, 122463. [CrossRef]
47. varshoei, A.; Javid, E.; Rahmaninia, M.; Rahmany, F. The Performance of Alkylketene Dimer (AKD) for the Internal Sizing of Recycled OCC Pulp. *Lignocellulose* **2013**, *2*, 316–326.
48. Zhang, Q.; Han, X.; Pu, J. In situ chemosynthesis of TiO_2 nanoparticles to endow paper with high water-resistance and retention rate properties. *Appl. Phys. A* **2018**, *124*, 571. [CrossRef]
49. Yuan, Z.; Wen, Y. Enhancement of hydrophobicity of nanofibrillated cellulose through grafting of alkyl ketene dimer. *Cellulose* **2018**, *25*, 6863–6871. [CrossRef]
50. Li, L.; Neivandt, D. The mechanism of alkyl ketene dimer (AKD) sizing on cellulose model films studied by sum frequency generation vibrational spectroscopy. *Cellulose* **2019**, *26*, 3415–3435. [CrossRef]
51. Kumudinie, C. Polymer–Ceramic Nanocomposites: Interfacial Bonding Agents. In *Encyclopedia of Materials: Science and Technology*; Buschow, K.H.J., Cahn, R.W., Flemings, M.C., Ilschner, B., Kramer, E.J., Mahajan, S., Veyssière, P., Eds.; Elsevier: Oxford, UK, 2001; pp. 7574–7577. [CrossRef]
52. Xiang, B.; Jiang, G.; Zhang, J. Surface modification of TiO_2 nanoparticles with silane coupling agent for nanocomposite with poly(butyl acrylate). *Plast. Rubber Compos.* **2015**, *44*, 148–154. [CrossRef]
53. Zhao, J.; Milanova, M.; Warmoeskerken, M.M.C.G.; Dutschk, V. Surface modification of TiO_2 nanoparticles with silane coupling agents. *Colloids Surf. Physicochem. Eng. Asp.* **2012**, *413*, 273–279. [CrossRef]
54. Xie, Y.; Hill, C.; Xiao, Z.; Militz, H.; Mai, C. Silane coupling agents used for natural fiber/polymer composites: A review. *Compos. Part Appl. Sci. Manuf.* **2010**, *41*, 806–819. [CrossRef]
55. Pouran, H.; Pérez Colodrero, R.; Wu, S.; Hix, G.; Zakharova, J.; Zhang, H. Assessment of ATR-FTIR spectroscopy with multivariate analysis to investigate the binding mechanisms of Ag and TiO_2 nanoparticles to Chelex®-100 or Metsorb™ for DGT technique. *Anal. Methods* **2020**, *12*, 959–969. [CrossRef]
56. El-Sherbiny, S.; Morsy, F.; Samir, M.; Fouad, O.A. Synthesis, characterization and application of TiO_2 nanopowders as special paper coating pigment. *Appl. Nanosci.* **2014**, *4*, 305–313. [CrossRef]
57. Anwar, M.S.; Kumar, S.; Ahmed, F.; Arshi, N.; Seo, Y.A.; Lee, C.; Koo, B. One Step Synthesis of Rutile TiO_2 Nanoparticles at Low Temperature. *J. Nanosci. Nanotechnol.* **2011**, *12*, 1555–1558. [CrossRef]
58. Li, L.; Yan, J.; Wang, T.; Zhao, Z.-J.; Zhang, J.; Gong, J.; Guan, N. Sub-10 nm rutile titanium dioxide nanoparticles for efficient visible-light-driven photocatalytic hydrogen production. *Nat. Commun.* **2015**, *6*, 5881. [CrossRef] [PubMed]
59. Ekoi, E.J.; Gowen, A.; Dorrepaal, R.; Dowling, D.P. Characterisation of titanium oxide layers using Raman spectroscopy and optical profilometry: Influence of oxide properties. *Results Phys.* **2019**, *12*, 1574–1585. [CrossRef]
60. Mazza, T.; Barborini, E.; Piseri, P.; Milani, P.; Cattaneo, D.; Li Bassi, A.; Bottani, C.; Ducati, C. Raman spectroscopy characterization of TiO_2 rutile nanocrystals. *Phys. Rev. B Condens. MATTER Mater. Phys.* **2007**, *75*, 045416. [CrossRef]
61. Wypych, A.; Bobowska, I.; Tracz, M.; Opasinska, A.; Kadlubowski, S.; Krzywania-Kaliszewska, A.; Grobelny, J.; Wojciechowski, P. Dielectric Properties and Characterisation of Titanium Dioxide Obtained by Different Chemistry Methods. Available online: https://www.hindawi.com/journals/jnm/2014/124814/ (accessed on 11 June 2020).
62. Wang, W.; Gu, B.; Liang, L.; Hamilton, W.A.; Wesolowski, D.J. Synthesis of Rutile (α-TiO_2) Nanocrystals with Controlled Size and Shape by Low-Temperature Hydrolysis: Effects of Solvent Composition. *J. Phys. Chem. B* **2004**, *108*, 14789–14792. [CrossRef]
63. Tsai, W.-B.; Kao, J.-Y.; Wu, T.-M.; Cheng, W.-T. Dispersion of Titanium Oxide Nanoparticles in Aqueous Solution with Anionic Stabilizer via Ultrasonic Wave. *J. Nanoparticles* **2016**. Available online: https://www.hindawi.com/journals/jnp/2016/6539581/ (accessed on 1 November 2020). [CrossRef]
64. Mandzy, N.; Grulke, E.; Druffel, T. Breakage of TiO_2 Agglomerates in Electrostatically Stabilized Aqueous Dispersions. *Powder Technol.* **2005**, *160*, 121–126. [CrossRef]
65. Al-Wassil, A.I.; Al-Farhan, K.A.; Mukhalalati, M.; Mahfouz, R.M. Coordination Chemistry of Thenoyltrifluoroacetone 1-Synthesis and Characterization of In^{3+}-thenoyltrifluoroacetone Complex. *Spectrosc. Lett.* **1998**, *31*, 299–305. [CrossRef]
66. Ferenc, W.; Cristóvão, B.; Sarzyński, J. Magnetic, thermal and spectroscopic properties of lanthanide(III) 2-(4-chlorophenoxy) acetates, Ln(C8H6ClO3)3•nH2O. *J. Serbian Chem. Soc.* **2013**, *78*, 1335–1349. [CrossRef]
67. Ukken, M.P.; Ummathur, M.B. Synthesis and Characterization of Two Conjugated b-diketones and their Metal Complexes. *Arch. Appl. Sci. Res.* **2013**, *5*, 247–250.
68. Kumar, M.; Sharma, T.R. Synthesis, Characterization and Properties of Metal Complexes of Beta-diketonate Complexes. *Orient. J. Chem.* **2012**, *28*, 1827–1831. [CrossRef]
69. Wu, J.G.; Deng, R.W.; Chen, Z.N. Transition metal complexes of 2-thenoyltrifluoroacetone isonicotinoyl hydrazone. *Transit. Met. Chem.* **1993**, *18*, 23–26. [CrossRef]

70. Bagheri, S.; Shameli, K.; Abd Hamid, S.B. Synthesis and Characterization of Anatase Titanium Dioxide Nanoparticles Using Egg White Solution via Sol-Gel Method. *J. Chem.* **2012**. Available online: https://www.hindawi.com/journals/jchem/2013/848205/ (accessed on 4 November 2020). [CrossRef]
71. Vetrivel, V.; Rajendran, D.K.; Kalaiselvi, V. Synthesis and characterization of Pure Titanium dioxide nanoparticles by Sol-gel method. *Int. J. ChemTech Res.* **2015**, *7*, 1090–1097.
72. Wang, Z.; Lian, J.; Xiang, X.; Zu, X.; Wang, L. Preparation and characterization of polymer/inorganic nanoparticle composites through electron irradiation. *J. Mater. Sci.* **2006**, *41*, 405–410.
73. Pan, H.; Wang, X.; Xiao, S.; Yu, L.; Zhang, Z. Preparation and characterization of TiO_2 nanoparticles surface-modified by octadecyltrimethoxysilane. *Indian J. Eng. Mater Sci.* **2013**, *7*, 561–567.
74. León, A.; Reuquen, P.; Garín, C.; Segura, R.; Vargas, P.; Zapata, P.; Orihuela, P.A. FTIR and Raman Characterization of TiO_2 Nanoparticles Coated with Polyethylene Glycol as Carrier for 2-Methoxyestradiol. *Appl. Sci.* **2017**, *7*, 49. [CrossRef]
75. Zhuravlev, L.T. Concentration of hydroxyl groups on the surface of amorphous silicas. *Langmuir* **1987**, *3*, 316–318. [CrossRef]
76. Kotsokechagia, T.; Cellesi, F.; Thomas, A.; Niederberger, M.; Tirelli, N. Preparation of Ligand-Free TiO_2 (Anatase) Nanoparticles through a Nonaqueous Process and Their Surface Functionalization. *Langmuir* **2008**, *24*, 6988–6997. [CrossRef]
77. Seo, W.S.; Cho, N.S.; Ohga, S. Possibility of Hydrogen Bonding between AKD and Cellulose Molecules. *J. Fac. Agric. Kyushu Univ.* **2008**, *53*, 405–410. [CrossRef]
78. Pliev, T.N.; Karpov, O.N.; Glavati, O.L.; Popovich, T.D. Infrared spectroscopic analysis of high-molecular alkenylsuccinic anhydrides for succinic anhydride groupings. *J. Appl. Spectrosc.* **1973**, *18*, 71–75. [CrossRef]
79. Nishiyama, M.; Isogai, A.; Onabe, F. Structures of Alkenyl Succinic Anhydride(ASA) Components in ASA-Sized Papersheet. *Seni Gakkaishi* **1996**, *52*, 180–188. [CrossRef]
80. Candy, L.; Vaca-Garcia, C.; Borredon, E. Synthesis and characterization of oleic succinic anhydrides: Structure-property relations. *J. Am. Oil Chem. Soc.* **2005**, *82*, 271–277. [CrossRef]
81. Huang, P.; Zhao, Y.; Kuga, S.; Wu, M.; Huang, Y. A versatile method for producing functionalized cellulose nanofibers and their application. *Nanoscale* **2016**, *8*, 3753–3759. [CrossRef]
82. Ba-Abbad, M.M.; Kadhum, A.A.H.; Mohamad, A.B.; Takriff, M.S.; Sopian, K. Synthesis and Catalytic Activity of TiO_2 Nanoparticles for Photochemical Oxidation of Concentrated Chlorophenols under Direct Solar Radiation. *Int. J. Electrochem. Sci.* **2012**, *7*, 18.
83. Lopera-Valle, A.; Elias, A. Amine Responsive Poly(lactic acid) (PLA) and Succinic Anhydride (SAh) Graft-Polymer: Synthesis and Characterization. *Polymers* **2019**, *11*, 1466. [CrossRef] [PubMed]
84. Song, X.; Chen, F.; Liu, F. Preparation and characterization of alkyl ketene dimer (AKD) modified cellulose compo-site membrane. *Carbohydr. Polym.* **2012**, *88*, 417–421. [CrossRef]